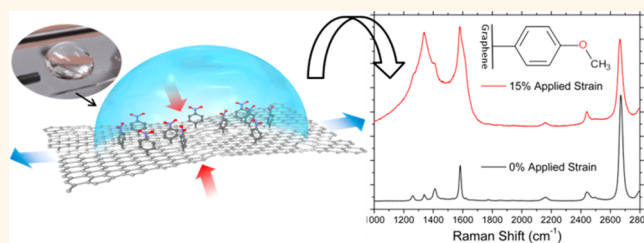# Enhanced Chemical Reactivity of Graphene Induced by Mechanical Strain

Mark A. Bissett,[†] Satoru Konabe,[‡] Susumu Okada,[‡] Masaharu Tsuji,[†] and Hiroki Ago[†,*]

[†]Institute for Materials Chemistry and Engineering, Kyushu University, Fukuoka 816-8580, Japan and [‡]Graduate School of Pure and Applied Sciences, University of Tsukuba, Tsukuba 305-8577, Japan

ABSTRACT Control over chemical reactivity is essential in the field of nanotechnology. Graphene is a two-dimensional atomic sheet of sp[2] hybridized carbon with exceptional properties that can be altered by chemical functionalization. Here, we transferred single-layer graphene onto a flexible substrate and investigated the functionalization using different aryl diazonium molecules while applying mechanical strain. We found that mechanical strain can alter the structure of graphene, and dramatically increase the reaction rate, by a factor of up to 10, as well as increase the final degree of functionalization. Furthermore, we demonstrate that mechanical strain enables functionalization of graphene for both p- and n-type dopants, where unstrained graphene showed negligible reactivity. Theoretical calculations were also performed to support the experimental findings. Our findings offer a simple approach to control the chemical reactivity of graphene through the application of mechanical strain, allowing for a tuning of the properties of graphene.

KEYWORDS: graphene · strain · chemical functionalization · reactivity · diazonium

Graphene has been the focus of an ever increasing amount of research due to its extraordinary properties, such as high charge carrier mobility, optical transparency, and mechanical flexibility.[1,2] By altering these properties, it will be possible to integrate graphene into a wide variety of applications, especially electronic devices. The tuning of graphene's electronic structure is made possible by a variety of methods including chemical functionalization,[3−5] mechanical strain,[6−9] and controlling the dimensions[10−12] and thickness[13] of graphene sheets, as well as applying an external electromagnetic field.[14,15]

Of these methods, chemical functionalization is the simplest and most versatile method for engineering the electronic structure of graphene and thus have control over its properties. One such reaction is the covalent attachment of aryl diazonium molecules *via* an electron transfer reaction.[16−21] This has been shown to shift the Fermi level of the graphene resulting in doping as well as introducing a band gap. However, to realize the full potential of graphene, it is necessary to have a high degree of control over the functionalization. It has been demonstrated that the rate and yield of functionalization can be affected by the supporting substrate[21] and the number of graphene layers,[16,17] as well as the presence of defects and grain boundaries.[22,23] It has also been shown theoretically that mechanical strain, which alters the electronic structure of graphene, can affect the reactivity of graphene for simple molecules such as hydrogen or metal nanoparticles.[24−27] Most recently, graphene that is deformed by contact with SiO$_2$ nanoparticles was experimentally shown to possess increased reactivity toward aryl diazonium functionalization, which was attributed to localized areas of increased curvature and strain.[28] Other carbon nanomaterials, such as carbon nanotubes or fullerenes, have long been known to have increased reactivity due to their curvature induced strain;[29,30] however, 2D materials such as graphene require further investigation.

Here, we experimentally demonstrate that mechanical strain can be used to dynamically tune the reactivity of graphene toward electron transfer chemistry, providing
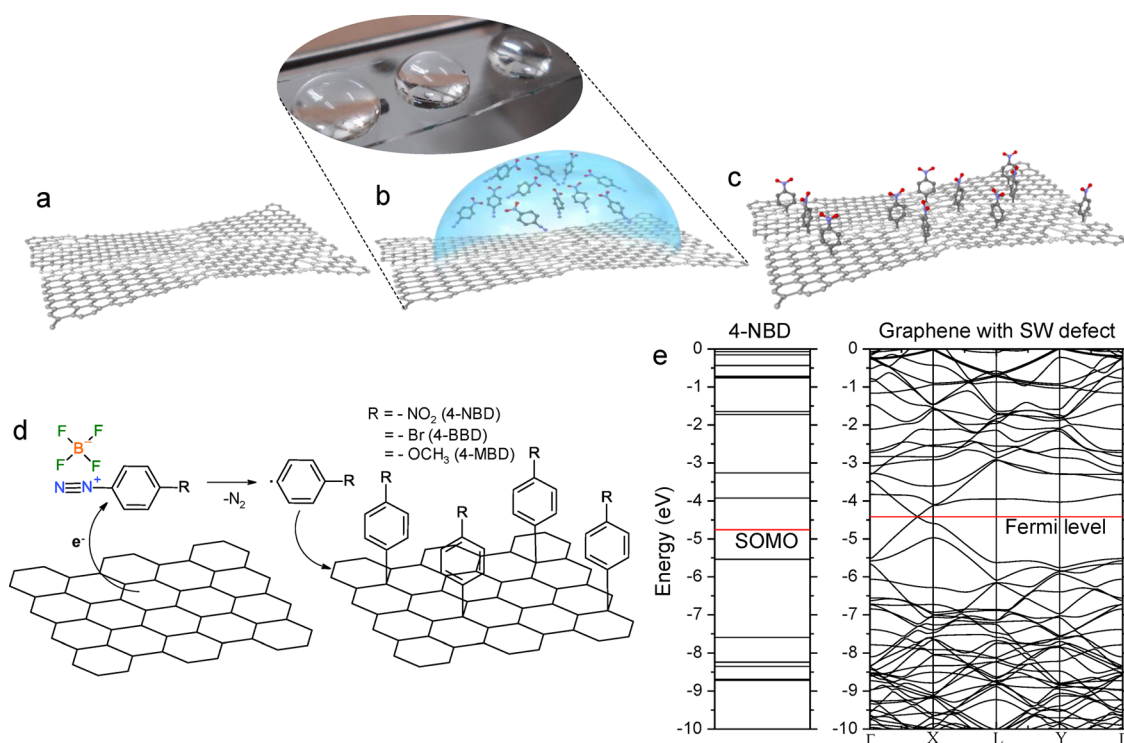
Figure 1. Schematic of strained graphene functionalization. (a) After being transferred to PDMS, the polycrystalline graphene is strained by elongation; due to the high Poisson's ratio of the PDMS, there is significant compression as well as tension applied. **(b)** After strain is applied, the aqueous solution of aryl diazonium salt is pipetted onto the graphene surface. The inset shows a photograph of several droplets on a graphene/PDMS substrate, allowing for several measurements for each strain value. As the graphene is only single-layer, it cannot be seen optically. **(c)** After functionalization, the solution is removed and the substrate rinsed and dried. Because of the increased reactivity of defect sites along boundaries, there is an increased concentration of functional molecules at these locations. **(d)** Schematic showing the functionalization of graphene by aryl diazonium molecules *via* an electron transfer mechanism. **(e)** Energy band diagram of 4-NBD and graphene containing a single Stone-Wales defect. During functionalization, an electron transfers from the π state just below the Fermi level of the graphene to the highlighted SOMO (single occupied molecular orbital) of the 4-NBD. The energies are measured relative to the vacuum level.

control over the level of doping and concentration of defects in the graphene. By applying strain to the graphene, it is possible to vastly increase both the rate of reactivity and the yield of functionalization. It is also demonstrated that unfavorable reactions that would not take place on relaxed graphene can be greatly enhanced by the application of strain to the graphene. In this instance, the application of mechanical strain acts as a 'catalyst' allowing the reaction to take place by reversibly altering the electronic structure of the graphene.

Large-area single-layer graphene was grown by chemical vapor deposition (CVD) before transfer to a flexible substrate, polydimethylsiloxane (PDMS). Mechanical strain is applied to the graphene by simply stretching the supporting substrate which causes reversible and damage-free deformation to the graphene lattice. The graphene is then functionalized by aryl diazonium molecules with differing functionalities, either electron donating or withdrawing, allowing for control over the type of doping of the graphene, as shown schematically in Figure 1(a–c). Raman spectroscopy is used to detect the degree of functionalization as well as doping by measuring the changes in relative Raman peak intensity and the shift in the

peak position, respectively. As a proof-of-concept for possible applications of this strain-enhanced reactivity, graphene was functionalized with both electron withdrawing and donating molecules on opposite areas, allowing for the construction of an in-plane p–n junction. Theoretical density functional theory (DFT) calculations are also used to explain the increased reactivity of the diazonium molecules toward the strained graphene.

RESULTS AND DISCUSSION

Chemical Functionalization of Flexible Graphene Substrates by Electron Transfer Chemistry. The two-step mechanism by which the aryl diazonium molecule covalently attaches to the graphene has been investigated previously[18,19] and is shown schematically in Figure 1d. Briefly, a delocalized electron from an occupied level is transferred from the graphene to an unoccupied level in the diazonium cation, shown in Figure 1e, rapidly forming an aryl radical. In this work, the three different aryl molecules used were 4-nitrobenzenediazonium (4-NBD), 4-bromobenzenediazonium (4-BBD) and 4-methoxybenzenediazonium (4-MBD). The aryl radical attaches to the graphene lattice converting the attachment site from a planar sp^2 to a tetrahedral sp^3

configuration. This covalent attachment can be detected by changes in the Raman spectrum. Changes to the spectrum include both an increase in the defect related D band from the covalent attachment, and a shift in peak position due to doping. Both the G and 2D peaks are shifted in frequency by doping, either up-shifting due to p-type doping or down-shifting for n-type, owing to the shift in the Fermi level at the K point.[31−33] Figure S1 shows the subsequent Raman spectra of graphene on PDMS with increasing functionalization time with 20 mM aqueous solution of 4-NBD. Both the G and 2D peaks upshift as functionalization time increases indicating that p-type doping has occurred, this is expected due to the electron withdrawing nature of the nitro moiety present on the 4-NBD and matches previous literature reports.[3,5,16,21,23]

During functionalization, the electron transfer and subsequent radical formation is the rate-limiting step and can be described by Gerischer-Marcus theory,[18,34] where the rate constant k_{ET} is defined in eq 1.

$$k_{ET} = v \int_{E_{redox}^D}^{E_F^G} \varepsilon_{red}(E) DOS_G W_{OX}(\lambda, E)\, dE \qquad (1)$$

$W_{OX}(\lambda, E)$ is the probability of a vacant state in the diazonium molecule, v is the frequency of electron transfer, ε_{red} is a proportionality factor and DOS_G is the density of states of the graphene. From this equation, we can see that the rate can be affected by altering the redox potential of the diazonium molecule used (E_{redox}^D) as well as altering the DOS and the Fermi level of the graphene (E_F^G, −4.56 eV for relaxed graphene[35]). The redox potential with respect to the vacuum level for the species used in this work have been determined previously from polarography as −5.15 eV (4-NBD), −5.08 eV (4-BBD) and −4.87 eV (4-MBD).[36] From eq 1 we would expect 4-NBD to have the highest reactivity due to the greatest difference in redox potential and the Fermi level of relaxed graphene, followed by 4-BBD and then 4-MBD as the least reactive. When we plot the rate of reactivity for these three molecules, as discussed later, on relaxed graphene we indeed observe this expected trend of decreasing reactivity.

Tuning the Reactivity by Mechanical Strain. Mechanical strain was applied by stretching the PDMS substrate, causing a distortion of the graphene lattice. The experimental apparatus used to apply mechanical strain is described in further detail in the Supporting Information (Figure S2). The applied strain is calculated as the ratio of increased length over original length [$(L_f − L_o)/L_o] \times 100\%$, where L_f and L_o are the final and original lengths, respectively. However, strain transfer between the polymer substrate and the graphene is not ideal and strain is lost due to inefficient interfacial transfer mechanisms such as slippage.[37,38] The strain may also not be homogenously distributed across large areas due to shear lag effects, leading to areas of localized

increased strain.[37,39] Theoretical calculations on the distribution of strain have also found that it is not homogenously dispersed across the graphene lattice, with some bonds undergoing localized strain 10−100 times larger than is applied externally.[24] This makes accurately determining the 'real' strain on the graphene difficult, so results presented here are the applied strain to the supporting substrate. The supporting substrate can also affect chemical reactivity due to substrate induced charge fluctuation in the graphene, forming charge unbalanced areas termed electron−hole puddles.[21] In the present work, the supporting substrate for all results is PDMS, as the substrate induced effect results from electron−hole puddle formation we can assume this remains constant even with increased strain due to the highly insulating nature of PDMS.

To measure the reactivity of the graphene, we plot the change in the Raman spectra, such as the relative peak intensity (I_D/I_G ratio), *versus* functionalization time as strain is applied. Figure 2 plots the reactivity of strained and unstrained graphene for each of the studied aryl diazonium species. Figure 2a shows the plot of the I_D/I_G ratio *versus* functionalization time for the nitro containing aryl diazonium (4-NBD). With no external applied strain, the I_D/I_G ratio of functionalized graphene on PDMS has a slope of 0.41 and reaches a saturation value of $\approx$0.35 after only 30 s before remaining constant thereafter. After applying mechanical strain of 8.7%, the slope increases to 0.63 and the saturation value increases to $\approx$0.45; this represents a $\approx$50% increase in reactivity. When the strain is further increased to 15%, the slope increases again to 0.82 and the saturation value to $\approx$0.6, an increase of 100% over the relaxed graphene. The spectra in Figure 2b illustrate the difference in spectra for the strained and unstrained sample after 30 s of functionalization time. Clearly there is a dramatic increase in D band intensity as well as increased upshift in peak position due to increased doping for both the G and 2D bands, both indicating the increased degree of functionalization has occurred due to the applied mechanical strain. For deconvolution of the spectra components, refer to the Supporting Information (Figure S6). As discussed previously, the nitro group present on 4-NBD is strongly electron withdrawing, and thus upon functionalization, the graphene is strongly p-type doped as seen by up-shifting of peak position.

Interestingly, when the unstrained sample was left for long periods of time (>24 h) to completely reach saturation, the I_D/I_G ratio remained constant. However, by applying strain, this saturation value can be increased considerably. The maximum coverage for aryl molecules attached to graphene has been calculated to be 11% ($\approx$4 $\times$ 10^{14} molecules/cm^2) in a para-position or (1, 4) configuration due to steric hindrance and long-range ordering.[18,40] However,
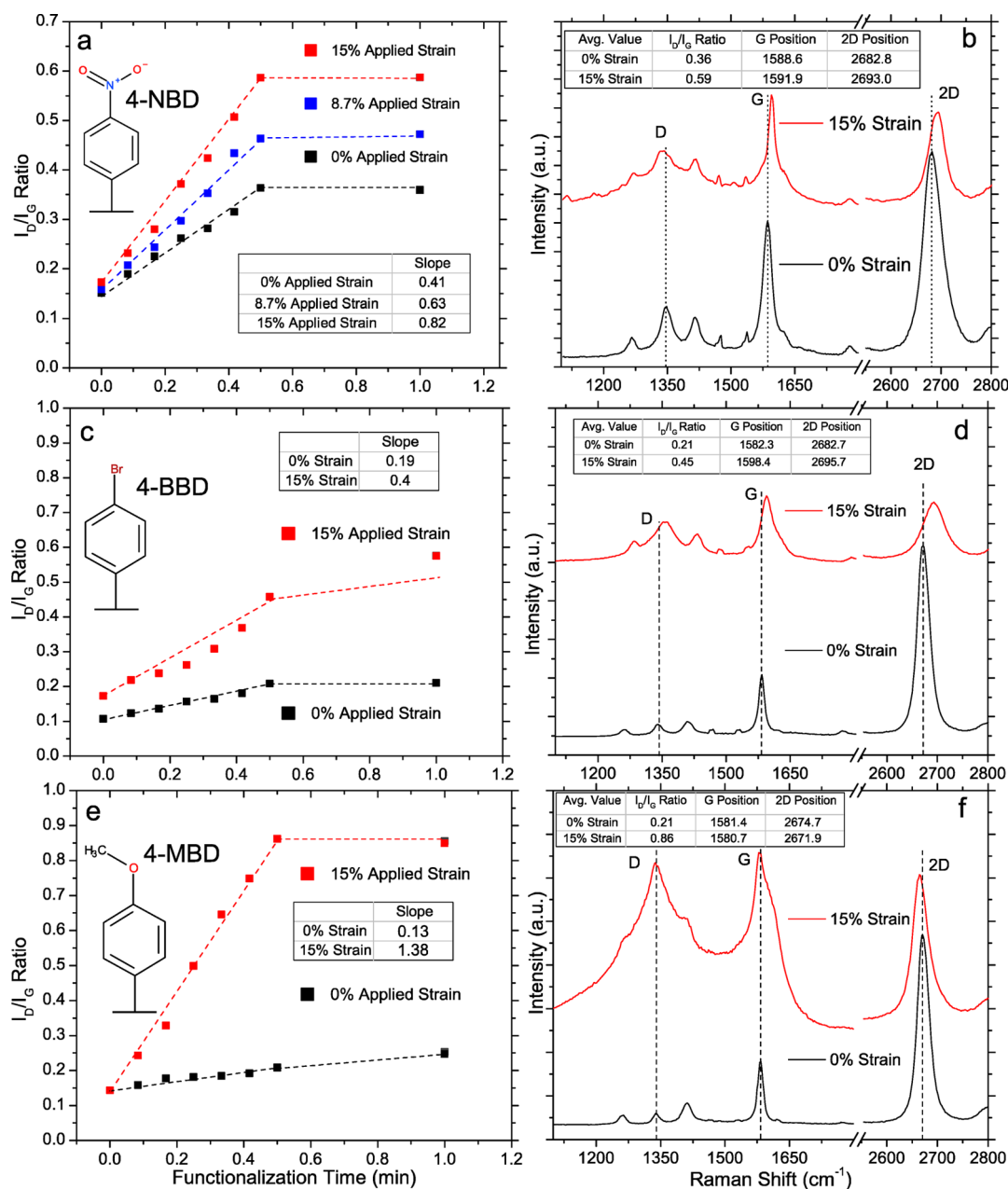
Figure 2. Plots of I_D/I_G ratio for unstrained and strained graphene with 20 mM solution of each aryl diazonium; 4-NBD (a), 4-BBD (c) and 4-MBD (e). Plots comparing the Raman spectra after 30 s of functionalization for both strained and unstrained graphene with each diazonium species; 4-NBD (b), 4-BBD (d) and 4-MBD (f). For each molecule, the addition of mechanical strain has increased both the rate of reaction as well as the final amount of attached molecules. For clarity, the results presented are the mean values; for values showing standard deviation and calculated error for slope and intercept, refer to the Supporting Information (Figures S3–S5).

this value depends on both the thermodynamic and kinetic regimes of the functionalization reaction. As we observe, this coverage value increases with strain; this indicates that the number of thermodynamically favorable configurations for aryl attachment is also increasing. This increased coverage could allow for sufficient yield to reach the values needed to open a practically applicable band gap in the graphene, a task difficult to accomplish on relaxed graphene. The inset table in Figure 2b presents the average values of I_D/I_G ratio, G position, and 2D position across the sample.

Figures 2(c) and 2(d) show the same increased reactivity of graphene toward the bromo containing molecule (4-BBD), also demonstrating an increase in slope of reactivity from 0.19 (0% strain) to 0.40 (15% strain) or approximately double. Again, we see that total functionalization value is also increased, as well as the peak shift due to increased p-type doping caused by the bromo functionality. This p-type doping caused by 4-BBD is also in agreement with previously reported literature.[41−43]

Figure 2e,f shows the results for the methoxy containing molecule (4-MBD). Because of the electron
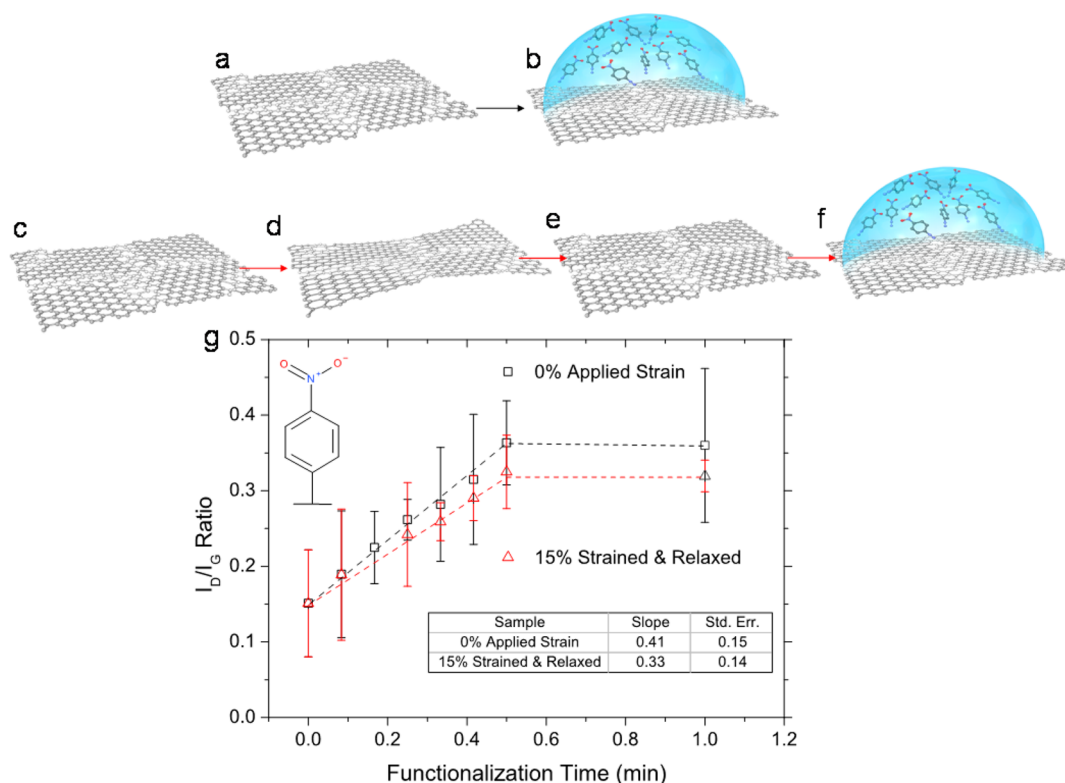
Figure 3. Schematic comparing the functionalization reaction for relaxed graphene (a and b) and graphene which is strained then relaxed before functionalization (c—f). (g) Plot comparing the reactivity of 4-NBD on unstrained graphene (seen in (a) and (b)) and graphene that is first strained to 15% then relaxed (seen in (c—f)). The slope is seen to be within standard error for both samples, indicating that the increased reactivity is not attributed to damage but instead distortion of the graphene lattice. The dashed line is added to guide the eye.

donating nature of methoxy moieties and the relative redox potential of 4-MBD to unstrained graphene, the rate of reaction is very low with a slope of only 0.13 and saturation has not occurred in the same time frames as the other molecules. However, after applying 15% strain, the rate of reaction is drastically improved, with a slope of 1.38 or a 10-fold increase in reactivity and the saturation value is ≈0.9. Figure 2f illustrates the dramatic difference in spectra when comparing unstrained graphene and strained graphene that have been functionalized for 30 s. In the highly functionalized spectra, the D band becomes broad due to overlap with neighboring PDMS peaks, as well as overlap with increased intensity diazonium specific peaks (1400 and 1440 cm^{-1}).[16] The enhanced D band is clearly seen by the deconvolution of the Raman spectrum, as shown in Supporting Information (Figure S6). The electron donating methoxy functionality on 4-MBD has previously been shown to produce n-type doped graphene[44] and a downshift in Raman peak position is observed in this work also indicating n-type doping. However, despite the large degree of functionalization, the overall down-shift in peak position due to n-type doping is quite small (1—3 cm^{-1}) due to the nonadiabatic Kohn anomaly, which causes peak shift to be only minor for n-type doping.[32,33,45]

To ensure that the increased reactivity observed is due to distortion of the graphene lattice and not damage being caused to the graphene such as tears, which would also increase the reactivity, a sample of graphene on PDMS was strained to 15% and then relaxed back to its original dimensions before being functionalized with 4-NBD. If the mechanical strain was sufficient to damage the graphene by causing tears or inducing other defects, we would expect that the strained and then relaxed graphene have similar reactivity to the 15% strained sample seen in Figure 2a,b. However, we can see that in Figure 3 that the strained then relaxed substrate exhibits reactivity that is similar to the unstrained sample; this confirms that strain is necessary for the increased reactivity and is not the result of damage. The lack of increased reactivity indicates that the level of strain applied (15%) allows for reversible, and damage free strain to be applied to the graphene. This also matches previous work where mechanical strain was shown not to induce defects in graphene until excessively high strain values are used.[2,23,37,39]

Theoretical Calculations. To explain the strain dependent increased reactivity, density functional theory (DFT) calculations were used. When external stress is applied to graphene, the orbital hybridization of the carbon atoms is affected, causing the formation of an extended π orbital with a localized electron (p$_z$ orbital)
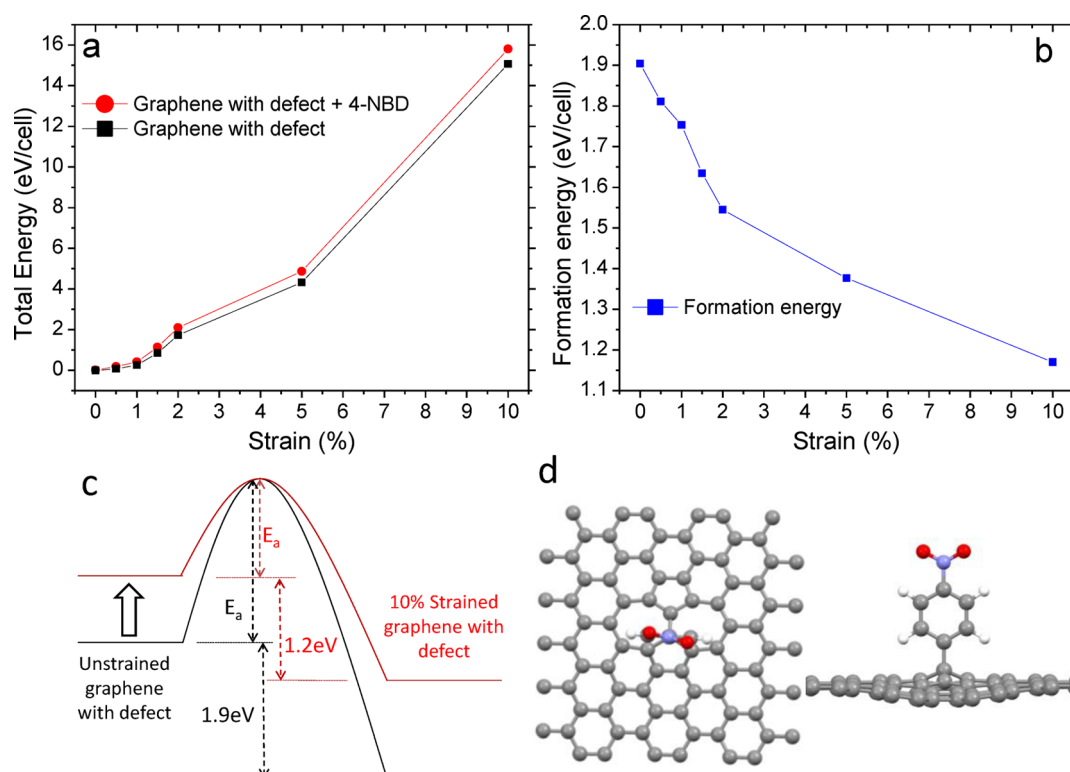
Figure 4. (a) Calculated total energy of graphene containing a Stone-Wales defect as well as 4-NBD functionalized graphene. (b) Calculated formation energy of 4-NBD functionalized graphene. The formation energy is defined as the difference between the functionalized complex plus the free nitrogen and the individual starting components (Formation Energy = 4-NBD_Graphene complex + N_2 − Graphene − 4-NBD). (c) Energy level diagram illustrating how the increased total energy of strained graphene leads to a decrease in the activation energy and an increase in reactivity. (d) Molecular image of optimized structure used for calculations showing 4-NBD functionalized graphene with a Stone-Wales defect.

available to form a covalent bond perpendicular to the graphene.[24,46] This extra electron availability is ideal for diazonium functionalization and can explain the increased reactivity observed experimentally in Figure 2. The charge density can also be altered by external strain,[46] and this may alter the charge transfer between the graphene and the diazonium molecule, leading to an increased rate of reactivity. Previous theoretical calculations on deformed graphene showed that as strain was increased the total energy of the graphene was also increased;[27,28,47] this increased total energy leads to increased reactivity of the graphene.

As the graphene used in this work is polycrystalline, we must also consider the effect of domain boundaries on the reactivity of graphene under mechanical strain. For wide scale roll-to-roll production, polycrystalline graphene is the most likely candidate, and thus, understanding the behavior of these domain boundaries is of paramount importance. Domain boundaries are typically thought of as detrimental to graphene's excellent properties; however, their presence also allows unique behavior that can be exploited.[48−50] Typically domain boundaries consist of a wide variety of defective structures,[51] but the most common is alternating pentagon-heptagon (5−7) rings which is similar in structure to the Stone-Wales defect. When we calculate the total energy of graphene using density functional

theory, containing a Stone-Wales defect, while undergoing strain, we find the energy increases with tensile strain, as shown in Figure 4a, in agreement with previous reports.[27,28,47] As discussed, this increased energy comes from destabilization of the graphene and leads to increased reactivity. This defect containing graphene is a more accurate approximation of the polycrystalline graphene used for our experimental results than the defect-free ideal graphene investigated previously. If we compare the total energy of the graphene containing a Stone-Wales defect as well as the aryl diazonium and N_2 molecules, in this case 4-NBD was used, the formation energy of the functionalized complex can be calculated, seen in Figure 4b. As strain is increased, we see a decrease in the formation energy; this will then decrease the energy gap between the initial and transition states, leading to the observed increase in reactivity. In this proposed model, we assume that the transition state energy remains similar for both strained and unstrained systems; we believe that this is a plausible assumption as the strain should alter the initial electron transfer step but not the subsequent transition state. The proposed energy level diagram is shown schematically in Figure 4c. The optimized structure showing the 4-NBD molecule attached to the Stone-Wales defect on the graphene is shown in Figure 4d. When similar calculations are
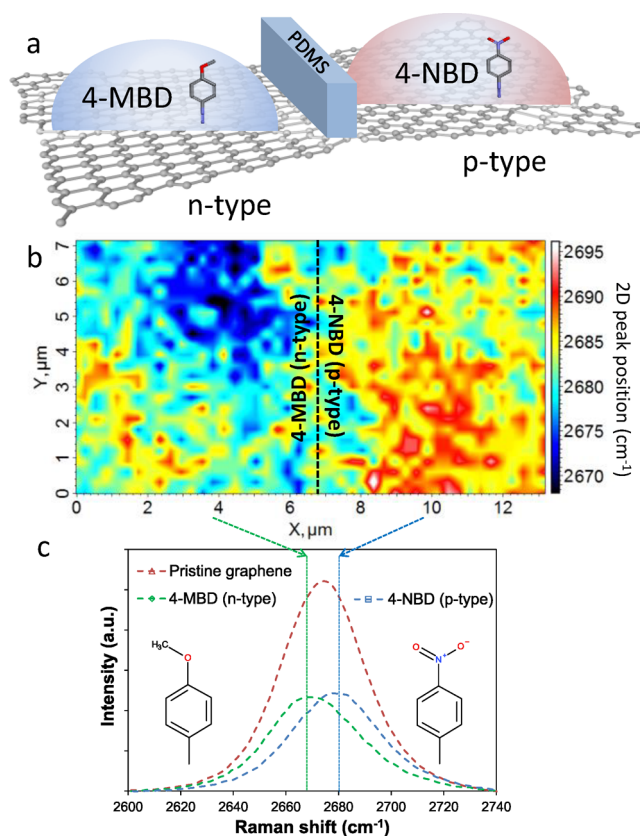
Figure 5. (a) Schematic showing graphene on PDMS was strained to 15% and then divided by using a PDMS mask, with one side being functionalized using 4-MBD (1 min), while the other side is functionalized with 4-NBD (1 min). This produces an interface where one side is p-type doped and the other n-type. (b) By mapping the Raman spectra at the interface, we can see that on one side the 2D peak position has downshifted due to n-type doping, while the other side has up-shifted due to p-type doping. (c) The Raman spectra of the 2D region are compared for pristine graphene (red), 4-MBD graphene (green), and 4-NBD graphene (blue). The 2D band intensity is decreased significantly for both doping types, and we see a downshift in position for the 4-MBD doped side matched by an upshift on the 4-NBD side, indicating that a p—n interface has been created.

performed for pristine graphene, it is found that the binding energy is significantly lower than that for the graphene with defects and there is no clear strain dependence (see Supporting Information Figure S7), indicating the importance of domain boundaries and defects in the reactivity of graphene. Although calculations indicate that ideal graphene exhibits no strain dependence, in reality nearly all graphene produced experimentally will possess some degree of defects, wrinkles or other imperfections from the growth or transfer processes making the strain enhanced functionalization applicable.

Synthesis of In-Plane p—n Junction. The method presented here allows for a dynamic tuning of the strain and thus a wide degree of control over the final degree of functionalization, essential for device integration. With the use of a combination of mechanical strain and chemical functionalization, it may be possible to create highly functionalized in-plane p—n junctions on graphene for use in electronic devices. When two areas of a single sheet of strained graphene are functionalized with both 4-NBD (p-type) and 4-MBD (n-type), it is possible to create an interface of p- and n-type doped graphene. With the use of Raman mapping to measure

the peak position, a measure of doping, it was possible to create such a junction, as shown in Figure 5. Further Raman mapping results are included in the Supporting Information (Figures S9, S10). Each side was functionalized for 1 min while 15% strain was applied; this is shown schematically in Figure 5a and then a Raman map was obtained of the interface (Figure 5b). After this bifunctionalization of the graphene, we see that the 2D peak position has downshifted on the n-type side while upshifting on the p-type side. The maximum difference in peak position is up to 20 cm^{-1}, representing a significant difference in charge carrier concentration.[33] Figure 5c illustrates the 2D spectrum from pristine graphene as well as typical spectra from both sides of the interface.

CONCLUSION

In summary, we have demonstrated here that chemical reactivity of graphene can be tuned by applying external strain *via* stretching of the supporting flexible substrate. The application of strain provided impressive increases in the rate of reactivity, by a factor of up to 10. It was also found that strain could be used as a catalyst to allow reactions that would otherwise not proceed, such as for electron donating functionalities

(4-MBD) which display very low reactivity on relaxed graphene, exhibiting a dramatic enhancement under strain. This also allowed the design of an in-plane p—n junction by doping graphene with different aryl functionalities, a reaction that would otherwise not be possible without strain tuning. Theoretical calculations supported the increased reactivity and it was attributed to distortions in the graphene lattice, especially potent at defect sites present along domain boundaries, due to destabilization of the graphene with increasing strain. This strain-catalyzed functionalization could be expanded to a wide variety of electron-transfer chemistries greatly increasing the functionalization options available for graphene and similar 2D materials.

METHOD

Graphene Synthesis and Transfer. Single-layer polycrystalline graphene was grown on copper foil by atmospheric pressure CVD as has been previously demonstrated.[52] In brief, the copper foil was first cleaned using isopropyl alcohol, then placed in a tube furnace with a 26 mm diameter quartz tube before annealing under hydrogen (10 sccm) and argon (300 sccm) atmosphere at 1000 °C for 60 min. Methane (0.5 sccm) was then introduced as the carbon source for 10 min before rapid cooling under the hydrogen and argon atmosphere. Large domain graphene was grown using the same growth conditions but lowering the methane flow rate to 0.15 sccm and increasing the growth time to 20 min. The graphene was then transferred from the copper foil to flexible PDMS substrates by drop coating liquid PDMS (Sylgard 184 Elastomer Kit, Dow Corning), with a base to curing agent ratio of 10:1 before curing. After the curing step, the copper foil was removed by etching in 1 M aqueous $FeCl_3$ leaving the graphene attached to the cured PDMS substrate.

Aryl Diazonium Functionalization. After graphene was transferred to the PDMS substrates, they were submerged in 20 mM aqueous solutions of aryl diazonium salt for varying amounts of time. The three molecules studied were 4-nitrobenzenediazonium tetrafluoroborate (4-NBD), 4-bromobenzenediazonium tetrafluoroborate (4-BBD) and 4-methoxybenzenediazonium tetrafluoroborate (4-MBD). Because of the volatility of diazonium solutions, fresh solutions were prepared and used immediately. For the strained measurements, the PDMS/graphene substrates were first elongated using a custom built strain apparatus and then functionalized as shown in Figure S2.

Raman Spectroscopy. Raman spectroscopy was performed on a Nanofinder 30 (Tokyo Instruments, Japan) using a laser excitation wavelength of 532 nm with a power of 5 mW and a 100× objective with a numerical aperture of 0.9. Raman maps were constructed by taking spectra spaced by 300 nm. It is possible to use Raman spectroscopy to calibrate the actual strain being exerted onto the graphene by measuring the strain induced peak shifts and fitting to the theoretical equations.[8,39,53] However, this method does not compensate for localized variations in strain, and samples a large area due to the spot size of the Raman laser. To attempt to compensate for this, the results presented here are the averages of several ($n = 15-60$) individual spectra taken from across the sample and the strain values presented are simply the applied strain as defined by the change in length of the substrate. For plots showing the mean as well as the standard deviation for each strain value, refer to Figures S3—S5.

Theoretical Calculations. All calculations were performed in the framework of density functional theory with local density approximation (LDA). To avoid the dipole effect from the periodic images of 4-NBD molecule, we adopted an effective screening medium method normal to the graphene layer. We used a $9 \times 5 \sqrt{3}$ lateral unit cell of graphene sheet with a Stone-Wales defect, seen in Figure 4d to investigate the energetics of adsorption of a 4-NBD molecule. We apply tensile strain up to 15% along the y-direction corresponding to the armchair direction of the graphene network; the lattice parameter for the super cell was fixed along the x-direction.

Conflict of Interest: The authors declare no competing financial interest.

REFERENCES AND NOTES

1. Novoselov, K. S.; Geim, A. K.; Morozov, S. V.; Jiang, D.; Zhang, Y.; Dubonos, S. V.; Grigorieva, I. V.; Firsov, A. A. Electric Field Effect in Atomically Thin Carbon Films. *Science* **2004**, *306*, 666–669.
2. Kim, K. S.; Zhao, Y.; Jang, H.; Lee, S. Y.; Kim, J. M.; Kim, K. S.; Ahn, J.-H.; Kim, P.; Choi, J.-Y.; Hong, B. H. Large-Scale Pattern Growth of Graphene Films for Stretchable Transparent Electrodes. *Nature* **2009**, *457*, 706–710.
3. Shih, C.-J.; Wang, Q. H.; Jin, Z.; Paulus, G. L. C.; Blankschtein, D.; Jarillo-Herrero, P.; Strano, M. S. Disorder Imposed Limits of Mono- and Bilayer Graphene Electronic Modification Using Covalent Chemistry. *Nano Lett.* **2013**, *13*, 809–817.
4. Shi, Y.; Kim, K. K.; Reina, A.; Hofmann, M.; Li, L.-J.; Kong, J. Work Function Engineering of Graphene Electrode *via* Chemical Doping. *ACS Nano* **2010**, *4*, 2689–2694.
5. Niyogi, S.; Bekyarova, E.; Itkis, M. E.; Zhang, H.; Shepperd, K.; Hicks, J.; Sprinkle, M.; Berger, C.; Lau, C. N.; deHeer, W. A.; *et al.* Spectroscopy of Covalently Functionalized Graphene. *Nano Lett.* **2010**, *10*, 4061–4066.
6. Pereira, V. M.; Castro Neto, A. H. Strain Engineering of Graphene's Electronic Structure. *Phys. Rev. Lett.* **2009**, *103*, 046801.
7. Guinea, F.; Katsnelson, M. I.; Geim, A. K. Energy Gaps and a Zero-Field Quantum Hall Effect in Graphene by Strain Engineering. *Nat. Phys.* **2010**, *6*, 30–33.
8. Huang, M.; Yan, H.; Heinz, T. F.; Hone, J. Probing Strain-Induced Electronic Structure Change in Graphene by Raman Spectroscopy. *Nano Lett.* **2010**, *10*, 4074–4079.
9. Levy, N.; Burke, S. A.; Meaker, K. L.; Panlasigui, M.; Zettl, A.; Guinea, F.; Neto, A. H. C.; Crommie, M. F. Strain-Induced Pseudo—Magnetic Fields Greater Than 300 Tesla in Graphene Nanobubbles. *Science* **2010**, *329*, 544–547.
10. Ritter, K. A.; Lyding, J. W. The Influence of Edge Structure on the Electronic Properties of Graphene Quantum Dots and Nanoribbons. *Nat. Mater.* **2009**, *8*, 235–242.
11. Todd, K.; Chou, H.-T.; Amasha, S.; Goldhaber-Gordon, D. Quantum Dot Behavior in Graphene Nanoconstrictions. *Nano Lett.* **2008**, *9*, 416–421.
12. Ryu, S.; Maultzsch, J.; Han, M. Y.; Kim, P.; Brus, L. E. Raman Spectroscopy of Lithographically Patterned Graphene Nanoribbons. *ACS Nano* **2011**, *5*, 4123–4130.
13. Ohta, T.; Bostwick, A.; Seyller, T.; Horn, K.; Rotenberg, E. Controlling the Electronic Structure of Bilayer Graphene. *Science* **2006**, *313*, 951–954.
14. Chuang, Y.-C.; Wu, J.-Y.; Lin, M.-F. Electric Field Dependence of Excitation Spectra in Ab-Stacked Bilayer Graphene. *Sci. Rep.* **2013**, *3*, 1368.
15. Sahu, B.; Min, H.; Banerjee, S. K. Effects of Edge Magnetism and External Electric Field on Energy Gaps in Multilayer Graphene Nanoribbons. *Phys. Rev. B* **2010**, *82*, 115426.

16. Koehler, F. M.; Jacobsen, A.; Ensslin, K.; Stampfer, C.; Stark, W. J. Selective Chemical Modification of Graphene Surfaces: Distinction between Single- and Bilayer Graphene. *Small* **2010**, *6*, 1125–1130.

17. Sharma, R.; Baik, J. H.; Perera, C. J.; Strano, M. S. Anomalously Large Reactivity of Single Graphene Layers and Edges toward Electron Transfer Chemistries. *Nano Lett.* **2010**, *10*, 398–405.

18. Paulus, G. L. C.; Wang, Q. H.; Strano, M. S. Covalent Electron Transfer Chemistry of Graphene with Diazonium Salts. *Acc. Chem. Res.* **2013**, *46*, 160–170.

19. Bekyarova, E.; Itkis, M. E.; Ramesh, P.; Berger, C.; Sprinkle, M.; de Heer, W. A.; Haddon, R. C. Chemical Modification of Epitaxial Graphene: Spontaneous Grafting of Aryl Groups. *J. Am. Chem. Soc.* **2009**, *131*, 1336–1337.

20. Zhang, H.; Bekyarova, E.; Huang, J.-W.; Zhao, Z.; Bao, W.; Wang, F.; Haddon, R. C.; Lau, C. N. Aryl Functionalization as a Route to Band Gap Engineering in Single Layer Graphene Devices. *Nano Lett.* **2011**, *11*, 4047–4051.

21. Wang, Q. H.; Jin, Z.; Kim, K. K.; Hilmer, A. J.; Paulus, G. L. C.; Shih, C.-J.; Ham, M.-H.; Sanchez-Yamagishi, J. D.; Watanabe, K.; Taniguchi, T.; *et al.* Understanding and Controlling the Substrate Effect on Graphene Electron-Transfer Chemistry *via* Reactivity Imprint Lithography. *Nat. Chem.* **2012**, *7*, 724–732.

22. Banhart, F.; Kotakoski, J.; Krasheninnikov, A. V. Structural Defects in Graphene. *ACS Nano* **2010**, *5*, 26–41.

23. Bissett, M. A.; Tsuji, M.; Ago, H. Mechanical Strain of Chemically Functionalized Chemical Vapor Deposition Grown Graphene. *J. Phys. Chem. C* **2013**, *117*, 3152–3159.

24. Andres, P. L. d.; Verges, J. A. First-Principles Calculation of the Effect of Stress on the Chemical Activity of Graphene. *Appl. Phys. Lett.* **2008**, *93*, 171915.

25. Xue, K.; Xu, Z. Strain Effects on Basal-Plane Hydrogenation of Graphene: A First-Principles Study. *Appl. Phys. Lett.* **2010**, *96*, 063103.

26. Kim, G.; Kawazoe, Y.; Lee, K.-R. Controlled Catalytic Properties of Platinum Clusters on Strained Graphene. *J. Phys. Chem. Lett.* **2012**, *3*, 1989–1996.

27. Boukhvalov, D. W.; Son, Y.-W. Covalent Functionalization of Strained Graphene. *ChemPhysChem* **2012**, *13*, 1463–1469.

28. Wu, Q.; Wu, Y.; Hao, Y.; Geng, J.; Charlton, M.; Chen, S.; Ren, Y.; Ji, H.; Li, H.; Boukhvalov, D. W.; *et al.* Selective Surface Functionalization at Regions of High Local Curvature in Graphene. *Chem. Commun.* **2013**, *49*, 677–679.

29. Srivastava, D.; Brenner, D. W.; Schall, J. D.; Ausman, K. D.; Yu, M.; Ruoff, R. S. Predictions of Enhanced Chemical Reactivity at Regions of Local Conformational Strain on Carbon Nanotubes: Kinky Chemistry. *J. Phys. Chem. B* **1999**, *103*, 4330–4337.

30. Park, S.; Srivastava, D.; Cho, K. Generalized Chemical Reactivity of Curved Surfaces: Carbon Nanotubes. *Nano Lett.* **2003**, *3*, 1273–1277.

31. Andrea C, F. Raman Spectroscopy of Graphene and Graphite: Disorder, Electron−Phonon Coupling, Doping and Nonadiabatic Effects. *Solid State Commun.* **2007**, *143*, 47–57.

32. Pisana, S.; Lazzeri, M.; Casiraghi, C.; Novoselov, K. S.; Geim, A. K.; Ferrari, A. C.; Mauri, F. Breakdown of the Adiabatic Born-Oppenheimer Approximation in Graphene. *Nat. Mater.* **2007**, *6*, 198–201.

33. Das, A.; Pisana, S.; Chakraborty, B.; Piscanec, S.; Saha, S. K.; Waghmare, U. V.; Novoselov, K. S.; Krishnamurthy, H. R.; Geim, A. K.; Ferrari, A. C.; *et al.* Monitoring Dopants by Raman Scattering in an Electrochemically Top-Gated Graphene Transistor. *Nat. Nanotechnol.* **2008**, *3*, 210–215.

34. Nair, N.; Kim, W.-J.; Usrey, M. L.; Strano, M. S. A Structure−Reactivity Relationship for Single Walled Carbon Nanotubes Reacting with 4-Hydroxybenzene Diazonium Salt. *J. Am. Chem. Soc.* **2007**, *129*, 3946–3954.

35. Yan, R.; Zhang, Q.; Li, W.; Calizo, I.; Shen, T.; Richter, C. A.; Hight-Walker, A. R.; Liang, X.; Seabaugh, A.; Jena, D.; *et al.* Determination of Graphene Work Function and Graphene-Insulator-Semiconductor Band Alignment by Internal Photoemission Spectroscopy. *Appl. Phys. Lett.* **2012**, *101*, 022105.

36. Elofson, R. M.; Gadallah, F. F. Substituent Effects in the Polarography of Aromatic Diazonium Salts. *J. Org. Chem.* **1969**, *34*, 854–857.

37. Young, R. J.; Gong, L.; Kinloch, I. A.; Riaz, I.; Jalil, R.; Novoselov, K. S. Strain Mapping in a Graphene Monolayer Nanocomposite. *ACS Nano* **2011**, *5*, 3079–3084.

38. Gong, L.; Kinloch, I. A.; Young, R. J.; Riaz, I.; Jalil, R.; Novoselov, K. S. Interfacial Stress Transfer in a Graphene Monolayer Nanocomposite. *Adv. Mater.* **2010**, *22*, 2694–2697.

39. Bissett, M. A.; Izumida, W.; Saito, R.; Ago, H. Effect of Domain Boundaries on the Raman Spectra of Mechanically Strained Graphene. *ACS Nano* **2012**, *6*, 10229–10238.

40. Jiang, D.-e.; Sumpter, B. G.; Dai, S. How Do Aryl Groups Attach to a Graphene Sheet? *J. Phys. Chem. B* **2006**, *110*, 23628–23632.

41. Dong, X.; Long, Q.; Wei, A.; Zhang, W.; Li, L.-J.; Chen, P.; Huang, W. The Electrical Properties of Graphene Modified by Bromophenyl Groups Derived from a Diazonium Compound. *Carbon* **2012**, *50*, 1517–1522.

42. Lim, H.; Lee, J. S.; Shin, H.-J.; Shin, H. S.; Choi, H. C. Spatially Resolved Spontaneous Reactivity of Diazonium Salt on Edge and Basal Plane of Graphene without Surfactant and Its Doping Effect. *Langmuir* **2010**, *26*, 12278–12284.

43. Farmer, D. B.; Golizadeh-Mojarad, R.; Perebeinos, V.; Lin, Y.-M.; Tulevski, G. S.; Tsang, J. C.; Avouris, P. Chemical Doping and Electron−Hole Conduction Asymmetry in Graphene Devices. *Nano Lett.* **2008**, *9*, 388–392.

44. Koehler, F. M.; Luechinger, N. A.; Ziegler, D.; Athanassiou, E. K.; Grass, R. N.; Rossi, A.; Hierold, C.; Stemmer, A.; Stark, W. J. Permanent Pattern-Resolved Adjustment of the Surface Potential of Graphene-Like Carbon through Chemical Functionalization. *Angew. Chem., Int. Ed.* **2009**, *48*, 224–227.

45. Lazzeri, M.; Mauri, F. Nonadiabatic Kohn Anomaly in a Doped Graphene Monolayer. *Phys. Rev. Lett.* **2006**, *97*, 266407.

46. Surya, V. J.; Iyakutti, K.; Mizuseki, H.; Kawazoe, Y. Modification of Graphene as Active Hydrogen Storage Medium by Strain Engineering. *Comput. Mater. Sci.* **2012**, *65*, 144–148.

47. Boukhvalov, D. W. DFT Modeling of the Covalent Functionalization of Graphene: From Ideal to Realistic Models. *RSC Adv.* **2013**, *3*, 7150–7159.

48. Yazyev, O. V.; Louie, S. G. Electronic Transport in Polycrystalline Graphene. *Nat. Mater.* **2010**, *9*, 806–809.

49. Wei, Y.; Wu, J.; Yin, H.; Shi, X.; Yang, R.; Dresselhaus, M. The Nature of Strength Enhancement and Weakening by Pentagon−Heptagon Defects in graphene. *Nat. Mater.* **2012**, *11*, 759–763.

50. Lahiri, J.; Lin, Y.; Bozkurt, P.; Oleynik, I. I.; Batzill, M. An Extended Defect in Graphene as a Metallic Wire. *Nat. Nanotechnol.* **2010**, *5*, 326–329.

51. Huang, P. Y.; Ruiz-Vargas, C. S.; van der Zande, A. M.; Whitney, W. S.; Levendorf, M. P.; Kevek, J. W.; Garg, S.; Alden, J. S.; Hustedt, C. J.; Zhu, Y.; *et al.* Grains and Grain Boundaries in Single-Layer Graphene Atomic Patchwork Quilts. *Nature* **2011**, *469*, 389–392.

52. Orofeo, C. M.; Hibino, H.; Kawahara, K.; Ogawa, Y.; Tsuji, M.; Ikeda, K.-i.; Mizuno, S.; Ago, H. Influence of Cu Metal on the Domain Structure and Carrier Mobility in Single-Layer Graphene. *Carbon* **2012**, *50*, 2189–2196.

53. Ding, F.; Ji, H.; Chen, Y.; Herklotz, A.; Dörr, K.; Mei, Y.; Rastelli, A.; Schmidt, O. G. Stretchable Graphene: A Close Look at Fundamental Parameters through Biaxial Straining. *Nano Lett.* **2010**, *10*, 3453–3458.